Elastic and Inelastic Scattering of 35-MeV Neutrons by 32S

I. 2. Elastic and Inelastic Scattering of 35-MeV Neutrons by ^{32}S

Ishimaru Y., Miyamoto S., Orihara H., Ishii K., Hosaka M., Zhong G., Nakagawa T., Terakawa A. Narita A.*, Niizeki T.**, and Ohnuma H.***

Cyclotron and Radioisotope Center, Tohoku University
** Department of Physics, Tohoku University*
*** Department of Physics, Tokyo Institute of Technology, Tokyo 152, Japan*

The nucleon-nucleus scattering is phenomenologically solved as the nucleon scattering by the Shrödinger equation,

$$-\frac{\hbar^2}{2M}\nabla^2\phi(r) + U_{opt}\phi(r) = E\phi(r), \quad (1)$$

M being the reduced mass of incident proton and target nucleus, with the optical potential

$$U_{opt} = V_{H.F.}(r, E) + \Delta V(r, E) + iW(r, E), \quad (2)$$

where the first term is the Hartree-Fock (H.F.), and the second and third ones are the dispersive contributions. The real part of U_{opt} consists of two terms, in which ΔV is connected to the imaginary potential by the dispersion relation;

$$\Delta V(r) = \frac{P}{\pi}\int_{-\infty}^{\infty}\frac{W(r, E')}{E' - E}dE', \quad (3)$$

where P denotes a principal value integral[1]. Thus, the $V_{H.F.}$ and ΔV terms may be obtained separately when we derive reliably the imaginary potential. Johnson and Mahaux have explained the energy dependence of the n-^{40}Ca mean field by a dispersive optical-model analysis[2].

The nucleon-nucleus scattering can be also used as a probe for estimating the size of charge-symmetry-breaking (CSB) potential. Winfield et al[3]. discussed CSB based on proton and neutron scattering data on self conjugate N=Z nuclei of ^{40}Ca , ^{32}S, ^{28}Si, and ^{12}C, comparing the real volume integrals of the proton (J_p) with those of the neutron (J_n). After corrected for Coulomb effects, averaged $(J_n\text{-}J_p)/A$ have some remaining evidences. However, their conclusions may suffer from the ambiguities to estimate the core-polarization effects.

On the basis of these results, we have discussed nucleon-^{28}Si and nucleon-^{12}C mean fields by a dispersive optical-model analyses, and suggested that the $(J_n\text{-}J_p)/A$ values for

^{28}Si might be due to core-polarization rather than charge symmetry breaking[4], while no significant difference was deduced for the case of the nucleon-^{12}C system[5].

In this report we discuss mainly nucleon-^{32}S mean field by a dispersive optical-model analysis. Since ^{32}S is one of the deformed nuclei with a quadrupole deformation parameter (β_2=0.283), we have to analyze assuming a rotational model, with the ground and 2^+ (2.23 MeV) states included, but no neutron inelastic scattering data are available at neutron energies above 26 MeV. Therefore, we measure elastic and inelastic neutron scattering data leading to the ground and 2^+ (2.23 MeV) states in ^{32}S at E_n=35 MeV, and analyze these data by the dispersive optical model for neutron and proton scattering data at energies in the 20-35 MeV range.

The real part of the optical potential thus obtained as a function of $E-E_F$, where E and E_F are, respectively, nucleon and Fermi energy, can be extrapolated from positive to negative energies where the potential describes the behavior of bound nucleons. It has been pointed out by Mahaux and Ngô[6] that an anomaly in the potential appeared near the Fermi surface. We discuss this point by comparing the energy dependence of the potential with those derived from single-particle (hole) energy for nucleons.

The experiment was carried out using AVF cyclotron and a neutron time of flight facility at the Cyclotron and Radioisotope Center, Tohoku University[7]. A neutron beam was produced by the ^{7}Li(p, n)^{7}Be (g.s.+ 0.429 MeV) reaction (Q = -1.644 MeV), and the energy spread was 600~700 keV, while the neutron flux was 4×10^5 /(μC·msr) in its magnitude. The natural sulfur target was formed as a cylinder (diameter 20 mm, height 75 mm, mass 38.96g). A sample neutron energy spectrum of the ^{32}S(n, n') reaction is shown in Fig.1.

The form of the optical potential adopted in the present analysis is given by

$$U_{opt} = -Vf\ (r, R, a) - iW_v f\ (r, R_v, a_v)$$
$$+ 4ia_s W_s \frac{d}{dr} f\ (r, R_s, a_s) + \left(\frac{h}{m_p c}\right)^2 V_{so}\, \vec{l}\cdot\vec{s}\, \frac{1}{r}\, \frac{d}{dr} f\ (r, R_{so}, a_{so}), \qquad (4)$$

where the form factor f is of a Wood-Saxon type

$$f\ (r, R_i, a_i) = \left[1 + \exp\left(\frac{r - R_i}{a_i}\right)\right]^{-1}$$, with potential radius R_i as; $R_i = \{1 + \beta_2 Y_2^0(\Omega)\} r_i A^{1/3}$,

where β_2 is static quadrupole deformation parameter. We have analyzed neutron data at E_n=14~40 MeV taken from Refs. 1, 8, 9 together with the presently obtained data for 35.3 MeV. Parameters for the spin-orbit term are fixed to those obtained by Woye et al.[10] through analyses for analyzing power data. They are V_{so}=5.66 MeV, r_{so}=0.76 fm, a_{so}=0.36 fm, and β^{so}_2=-0.56. Coupled-channel analyses (CC) are carried out by the code ECIS79 by Raynal[11]. The results of the potential search for neutron scattering at E_n=14.0, 14.83, 17.0, 20.0, 21.5, 21.6, 26.0, 30.3, 35.3 and 40.3 MeV are given in Table 1, and a sample of

simultaneous fitting to elastic and inelastic differential cross sections at E_n=35 MeV is shown in Fig. 2.

We define the volume integral of the optical potential $U(r, \Omega)$ as;

$$J/A = \frac{1}{A}\int U(r, \Omega)d\vec{r}\,, \qquad (5)$$

by which we are able to discuss less ambiguously independent of the fine structure of uncertainties for geometrical parameters. Imaginary surface and imaginary volume potentials listed in Table 1 were thus integrated for the following discussion. Figure 3 represents the energy dependence of these potentials for the n + ^{32}S system. Curves in the figure show parametrization by the functions suggested by Das and Finley[8], i.e.

$$J_{W_V}(E) = C_1\frac{(E - E_F)^4}{(E - E_F)^4 + C_2{}^4} \quad \text{and} \quad J_{W_S}(E) = C_3\frac{(E - E_F)^4 exp(C_4(E - E_F))}{(E-E_F)^4 + C_5{}^4}\,, \qquad (6)$$

where E_F is the Fermi energy (-12.1 MeV for the present case). The parameters for neutrons obtained by fitting the experimental data including inelastic scattering ones are:

C_1= -134 MeV·fm^3, C_2= 56.1 MeV, for J (W_V),
C_3= -205 MeV·fm^3, C_4= -2.02 x 10^{-2} MeV^{-1}, C_5= 9.05 MeV, for J (W_S).

Applying the dipersion relation in Eq (3), we find corresponding real parts:

$$J_{\Delta V_V}(E) = -C_1\cdot C_2\frac{(E - E_F)\left[(E - E_F)^2 + C_2{}^2\right]}{\sqrt{2}\left[(E - E_F)^4 + C_2{}^4\right]},$$

$$J_{\Delta V_S}(E) = \frac{2}{\pi}\times\int_0^{+\infty}\frac{\tilde{J}_{W_S}(y) - \tilde{J}_{W_S}(x)}{y^2 - x^2}dy \quad \text{and} \quad J_{\Delta V}(E) = J_{\Delta V_V}(E) + J_{\Delta V_S}(E). \qquad (7)$$

The energy dependence of these volume integrals calculated by Eq(7) with the coefficients listed above are illustrated in Fig. 4.

As for proton scattering on ^{32}S, reported in Refs. 12-14, we have performed similar analyses for the data at E_p = 15, 17.0, 18.24*, 19.0, 20.37*, 21.0, 23,0, 23.24*, 25.0, 26.55*, 29.64*, 35.2* and 65.0* MeV, where at E_p with * inelastic data had been reported. The coefficient in Eqs(6) and (7) obtained for protons are,

C_1= -66.8 MeV·fm^3, C_2= 44.9 MeV, for J (W_V),
C_3= -134 MeV·fm^3, C_4= -1.32 x 10^{-2} MeV^{-1}, C_5= 8.38 MeV, for J (W_S).

The real potential depths, which were obtained from CCBA analyses and consist of the sum of $V_{H.F.}$ and ΔV, seem to be different for n-^{32}S and p-^{32}S systems. In Fig. 5, the

difference is plotted as a function of the nucleon energy, showing that there is sizable evidence. The curve in the figure is [$J\Delta V$(for neutron)-$J\Delta V$(for proton)]/A, former of which is plotted in Fig. 4. Though experimental ambiguities are still large, the differences are interpreted by the difference of core-polarization between n-^{32}S and p-^{32}S.

The contribution of Hartree-Fock field to the real part of the empirically-obtained optical-potential is estimated by subtraction of $J\Delta V$ from JV(real). Energy dependence of $J(V_{\mathrm{H.F.}})$ is parametrized as following;

$$J(V_{\mathrm{H.F.}}) = -525 \times \exp\{-6.93\times10^{-3}(E-E_{\mathrm{F}})\} \quad (\mathrm{MeV\cdot fm^3}) \tag{8}$$

for neutrons, while it is

$$J(V_{\mathrm{H.F.}}) = -507\times\exp\{-7.81\times10^{-3}(E-E_{\mathrm{F}})\} \quad (\mathrm{MeV\cdot fm^3}) \tag{9}$$

for protons. Figures 6 and 7 illustrate depths of the real and Hartree-Fock potentials for neutrons and protons, respectively. Curves refer to the present results extended over the Fermi surface, the points near which are the bound potential depths for each particle and hole orbits indicated in the figure.

In conclusion, we have measured neutron elastic and inelastic scattering from ^{32}S at E_n=35 MeV, and analyzed these data by the dispersive optical model together with neutron scattering data from 14~40 MeV, and with the proton data in 15 through 65 MeV in order to evaluate core polarization effect. The $(J_n-J_p)/A$ values and their energy dependence are explained by difference of core polarization between n-^{32}S and p-^{32}S. The anomaly in the potential appearing near the Fermi surface was well described by the energy dependence of the real potential obtained in the present study.

References

1) Mahaux C. et al., Phys. Rep. **120** (1985) 1.
2) Johnson C. H. and Mahaux C., Phys. Rev. C **39** (1989) 415.
3) Winfield J. S. et al., Phys. Rev. C **33** 1986) 1.
4) Niizeki T. et al., CYRIC Annual Report (1989) p.10.
5) Miyamoto S. et al., CYRIC Annual Report (1992) p.1.
6) Mahaux C. and Ngô H., Phys. Lett. **B100** (1979) 285.
7) Orihara H. et al., Nucl. Instrum. and Methods **A257** (1987) 189.
8) Das P. K. and Finlay R. W., Phys. Rev. C **42** (1990) 1013.
9) Delaroche J. P. Wang Y. and Rapaport J., Phys. Rev. C **39** (1989) 391.
10) Woye E. et al., Nucl. Phys. **A394** (1983) 39.
11) Raynal J., the code ECIS79(unpublished).
12) Deleo R. et al., Nuovo Cimento **59A** (1980) 101.
13) Roy R., Lamontagne C. R. and Slobodrian R.J., Nucl. Phys. **A411** (1983) 1.
14) Kato S. and Okada K., Phys. Rev. C **31** (1985) 1616.

Table 1. Results of the CC analysis for neutron scattering.

r = 1.149 fm, a = 0.733 fm, a_s = 0.627 fm, r_V = 1.149 fm, a_V= 0.733 fm

E_n(MeV)	V(MeV)	W_V(MeV)	W_S(MeV)
14.0	52.1	0.0	6.60
14.83**	50.8	0.0	7.17
17.0	49.2	0.0	6.53
20.0**	48.8	1.67	6.03
21.5**	48.5	1.85	5.48
21.6	48.4	2.10	5.23
26.0	46.8	3.45	4.82
30.3	47.4	3.55	5.17
35.3**	46.0	3.93	4.54
40.3	44.2	6.58	3.87

** includes inelastic scattering data

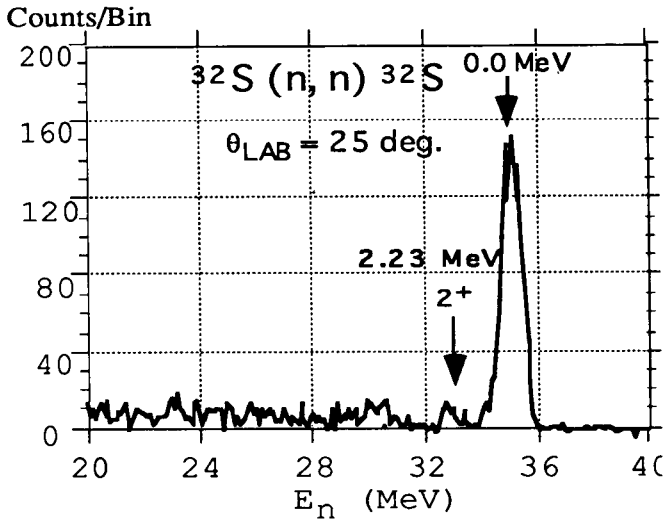

Fig. 1. A sample neutron energy spectrum of the ^{32}S(n,n') reaction

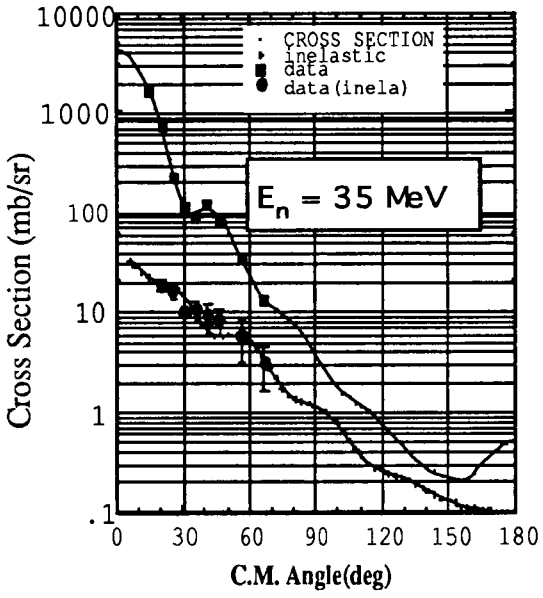

Fig. 2. Differential cross sections for elastic and inelastic scattering of 35 MeV neutrons from ^{32}S. The curves are CC fits.

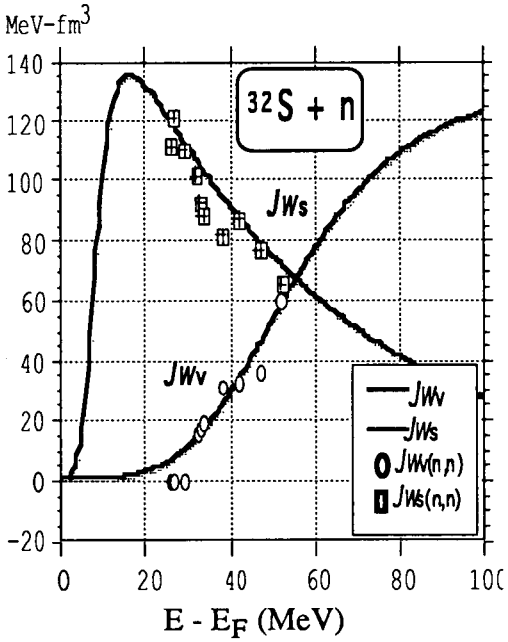

Fig. 3. Energy dependence of volume integrated imaginary parts. Lines are fitted results by Eq(6)

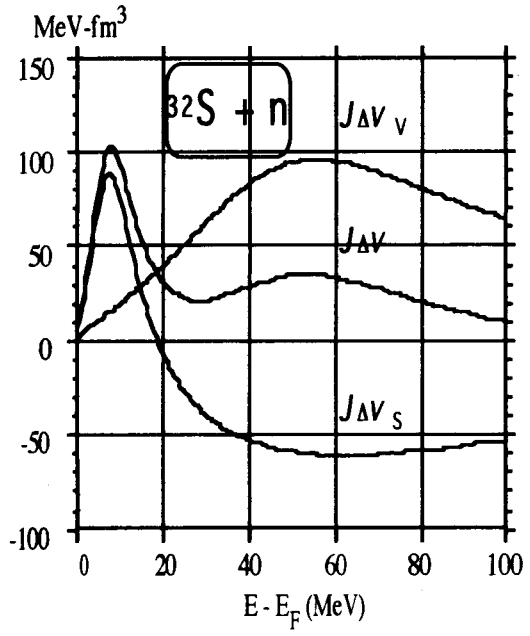

Fig. 4. Energy dependence for the volume integral of $J\,\Delta V_V$ and $J\,\Delta V_S$ in n + ^{32}S system.

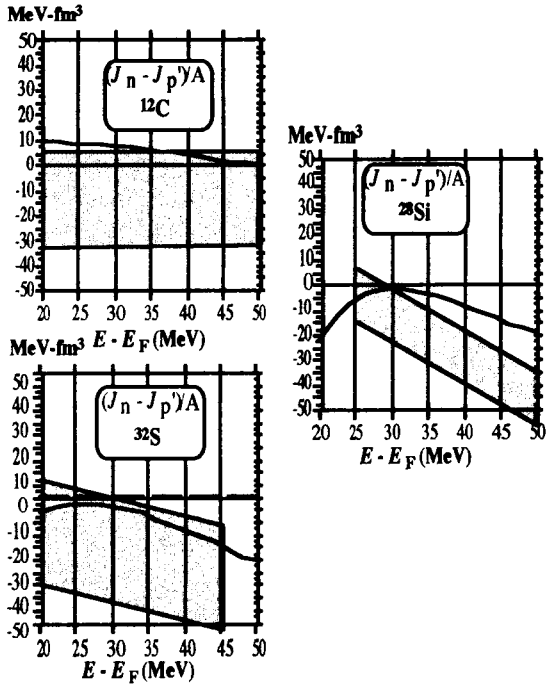

Fig. 5. Differences of the real volume integrals per nucleon.

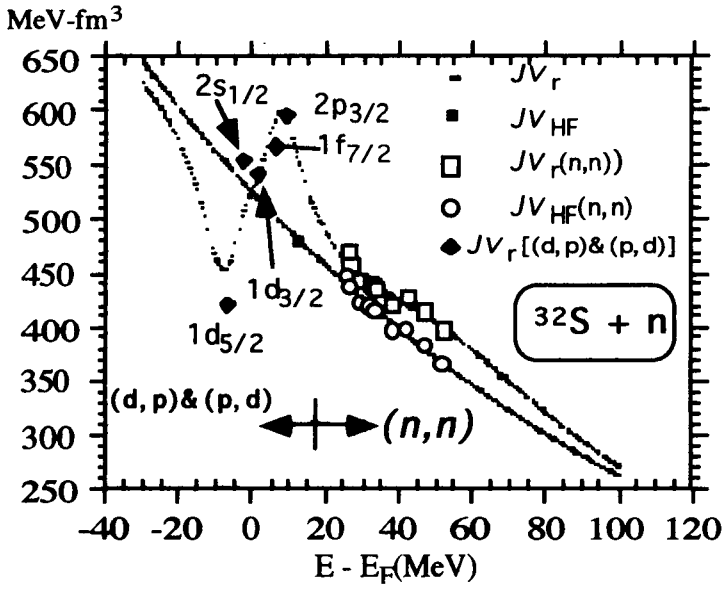

Fig. 6. Depths of "total" real and Hartree-Fock(dotted curve) potentials for neutrons. Lines are present results extended over the Fermi surface, the points near which are the bound potential depths for each neutron particle and hole orbit indicated in the figure.

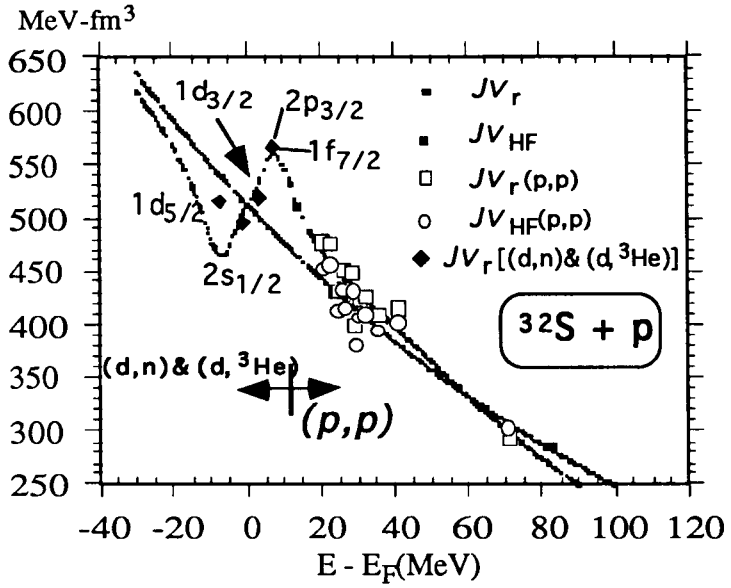

Fig. 7. Same with Fig. 6 but for protons.